Supporting information

Deborah number-dependent transition from homogeneity to heterogeneity

*Dan Xu[1], Yang Yang[1], Lukas Emmerich[2], Yong Wang[3], Kai Zhang[1]**

Address

1 Sustainable Materials and Chemistry, Department of Wood Technology and Wood-based Composites, Georg-August-University of Göttingen, Büsgenweg 4, D-37077 Göttingen, Germany.

2 Department of Wood Biology and Wood Products, Georg-August-University of Göttingen, Büsgenweg 4, D-37077 Göttingen, Germany.

D-37077 Göttingen, Germany.

3 Laboratory for Fluid Physics, Pattern Formation and Biocomplexity, Max Planck Institute for Dynamics and Self-Organization, Am Faßberg 17, D-37077 Göttingen, Germany.

*Corresponding author. E-mail: kai.zhang@uni-goettingen.de

This file includes:

The volatility evaluation of various media

The liquid phase velocity is small compared to the moist air velocity, which means advective transport rate (in the inner part of hydrogel) is lower than diffusive transport rate (on the interface of hydrogel/air). Therefore the water velocity in hydrogel is determined by gas phase pressure gradient (based on Dancy' law). Under the assumption that all hydrogels are of similar porous structures, the whole evaporation process is mainly dominated by the volatility of media.

Here, three media were applied in the system, including the original sodium hydroxide, borax-NaOH buffer (pH = 10.00) (buffer), a faster evaporation system containing 10% ethanol and a slower evaporation system containing 5% glucose. To quantitatively describe the volatility difference between these media, an approximate calculation was applied based on Henry's law and Raoult's low, and the saturated vapor pressure was set as the evaluation criterion. Under constant ambient pressure and temperature, the volatility and the saturated vapor pressure is positive correlation, which means that the liquid of high saturated vapor pressure allows for easier transition from liquid to gas. Here, the temperature was set as 293 K and the ambient pressure was 1 atm.

To simplify things, we would use the saturated vapor pressure of water to refer to that of buffer solution. Thus, the saturated vapor pressure of the system is around 2.34 kPa.

As for the faster evaporation system containing 10% ethanol, the Henry's law was applied.

$$P = P_{water} + P_{ethanol} = x_{water}P^0_{water} + x_{ethanol}P^0_{ethanol} \quad (1.1)$$

Here, x refers to the molar percentage of chemicals, and the P^0 means the saturated vapor pressure of chemicals. Herein, the saturated vapor pressure of the medium is 2.69 kPa.

As for the slower evaporation system containing 5% glucose, the Raoult's law was applied.

$$P = P^0_{water} - \Delta P = x_{water}P^0_{water} \quad (1.2)$$

Here, ΔP is the decreased vapor pressure of medium due to colligative properties of glucose solution. Thus, the saturated vapor pressure of the medium is 2.22 kPa.

In brief, the order of evaporated speed can be regarded as:

10% ethanol > buffer > 5% glucose

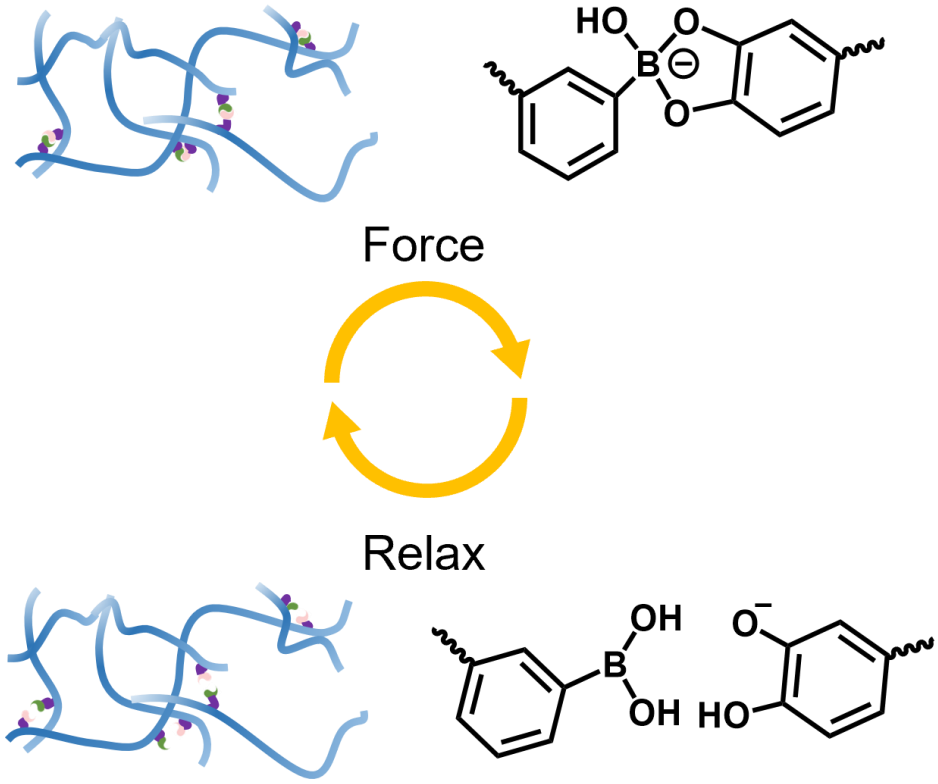

Fig S1. The energy dissipation mechanism of dynamic hydrogel in the process of uniaxial stretching via the reconstruction of non-covalent bonding.

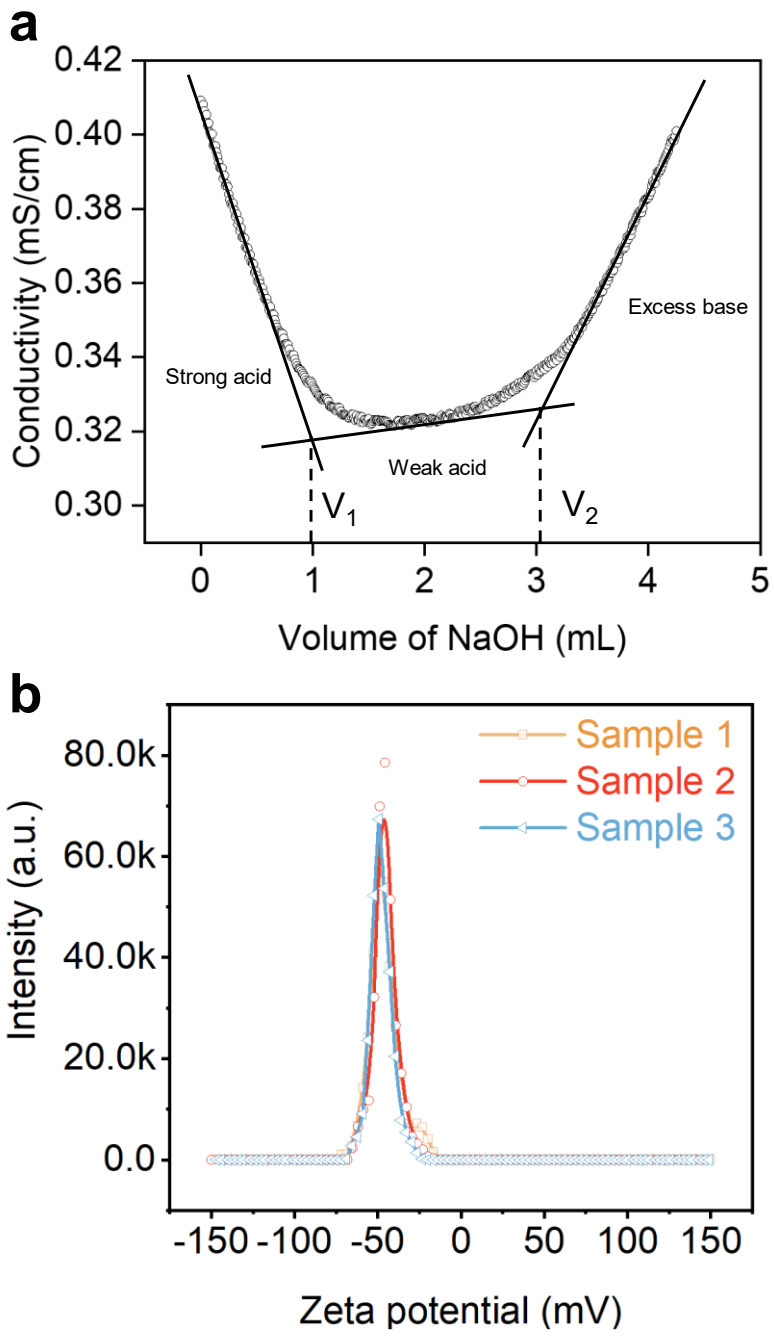

Fig S2. a) Typical conductometric titration curve of CNCs; b) Zeta potential distribution of CNCs. (N = 3)

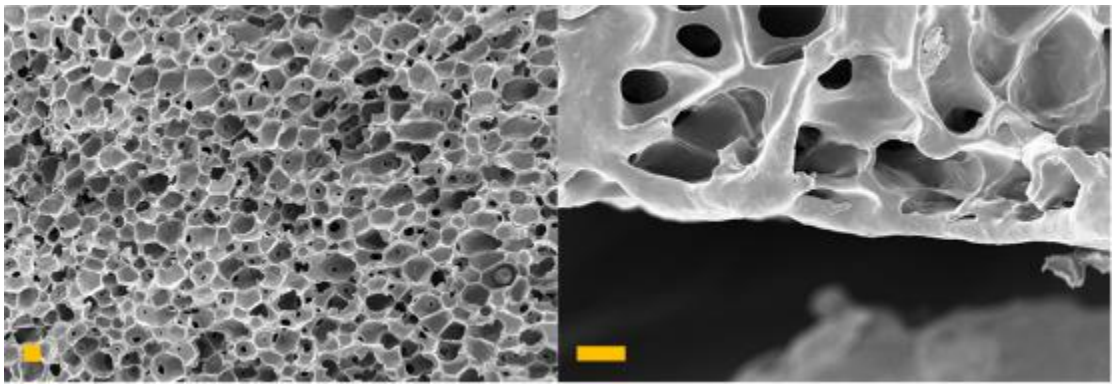

Fig S3. SEM images of virgin CNC hybrid hydrogel after freeze-drying without stretching and air-drying. Left: inner part; Right: outer part. Scale bar: 10 μm.

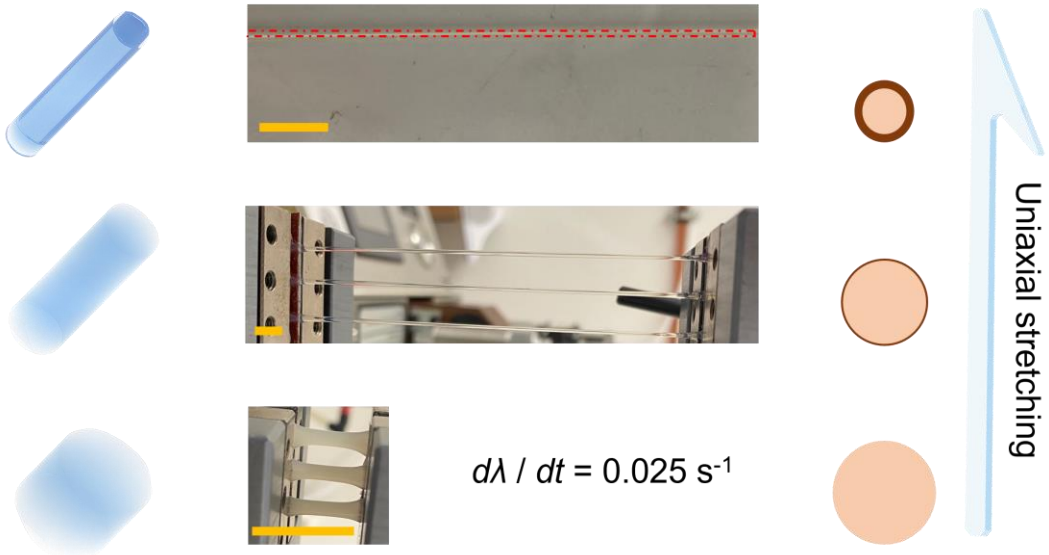

Fig S4. Schema of plants inspired spontaneously formed core-sheath structural hybrid fibers. (Scale bar: 5 mm)

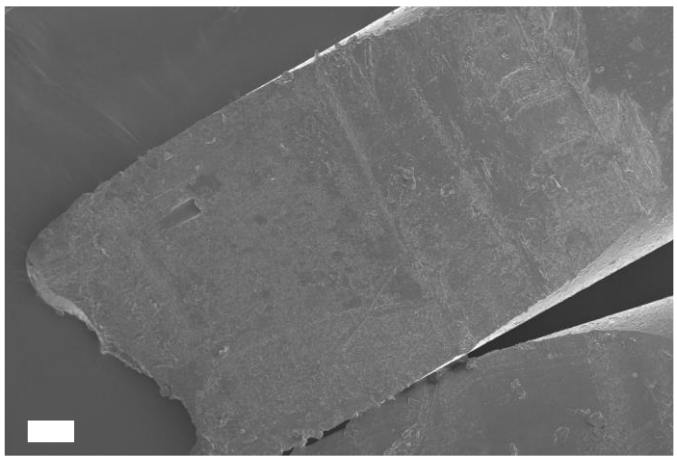

Fig S5. SEM image of the bevel section in the xerogel fiber. Scale bar:100 μm.

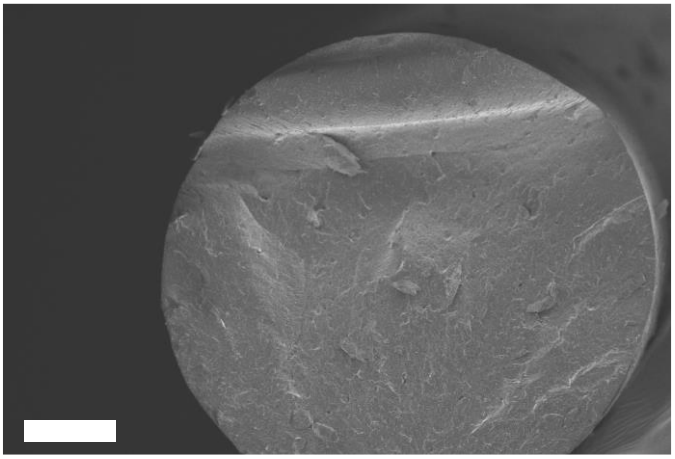

Fig S6. SEM image of cross section of a xerogel fiber. Scale bar:100 μm.

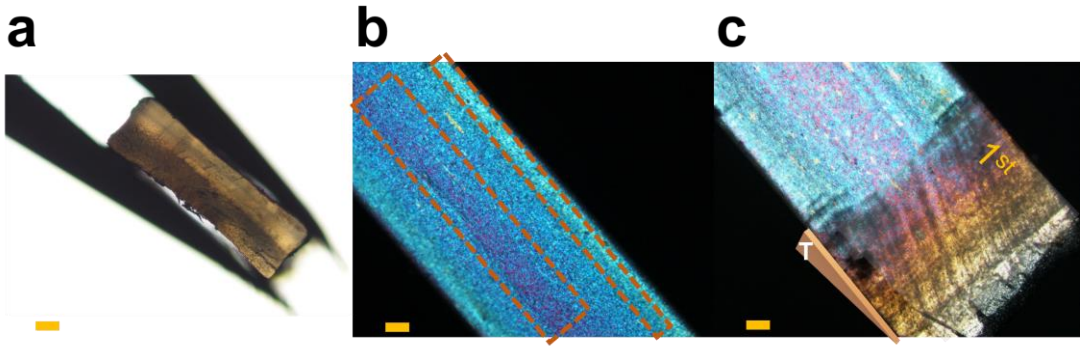

Fig S7. Optical and POM images of CNC hybrid xerogel films. a) Optical images of xerogel film cross section; and the POM images of bevel xerogel fibers, including b) Surface and c) Bevel section. Scale bar: 100 μm.

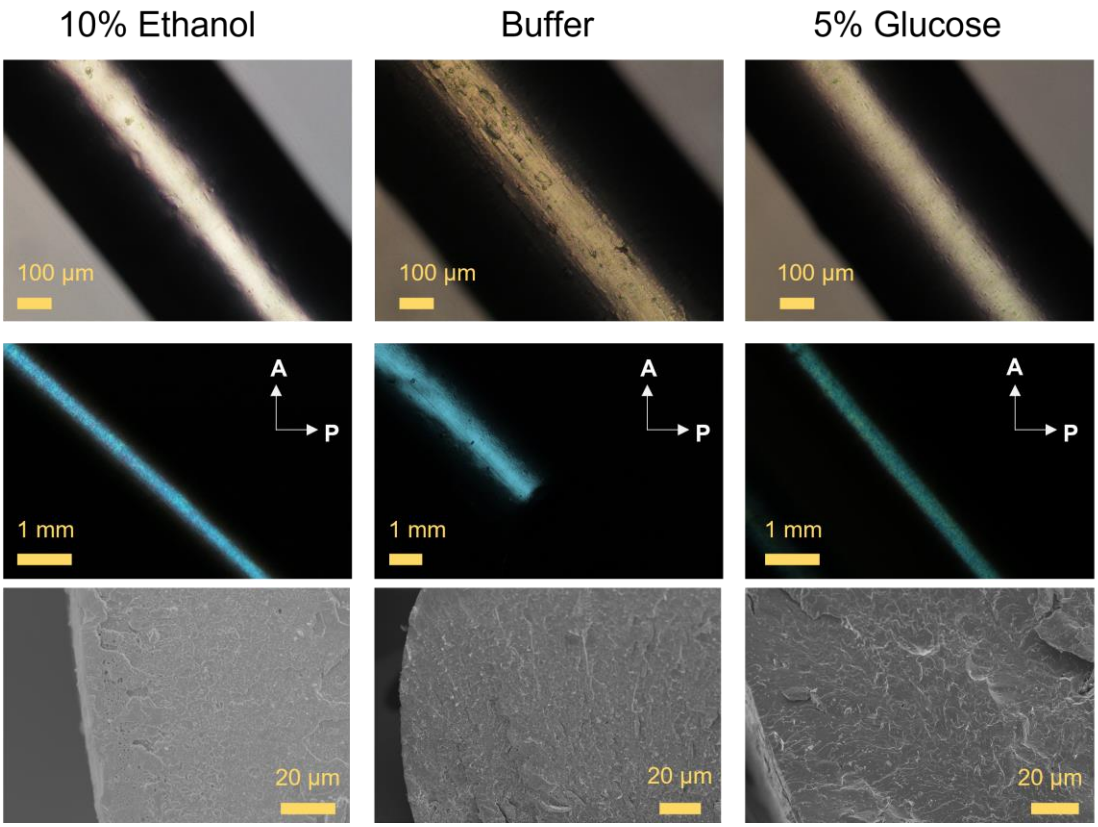

Fig S8. top) Optical microscopy images, middle) Polarized microscopy images and bottom) SEM images of various obtained xerogel fibers.

Table S1. The physics parameters used to simulate the air drying of hydrogel fibers[1-5]

293.15 [K]	Ambient temperature
0.05 [m/s]	Freestream velocity
0.3	Ambient relative humidity
0.3	Irreductible liquid phase saturation
0.59	Porosity
0.98*1e-12 [m^2]	Permeability
0.8 [W/(m*K)]	Porous matrix thermal conductivity
6500 [J/(kg*K)]	Porous matrix heat capacity
1200 [kg/m^3]	Porous matrix density

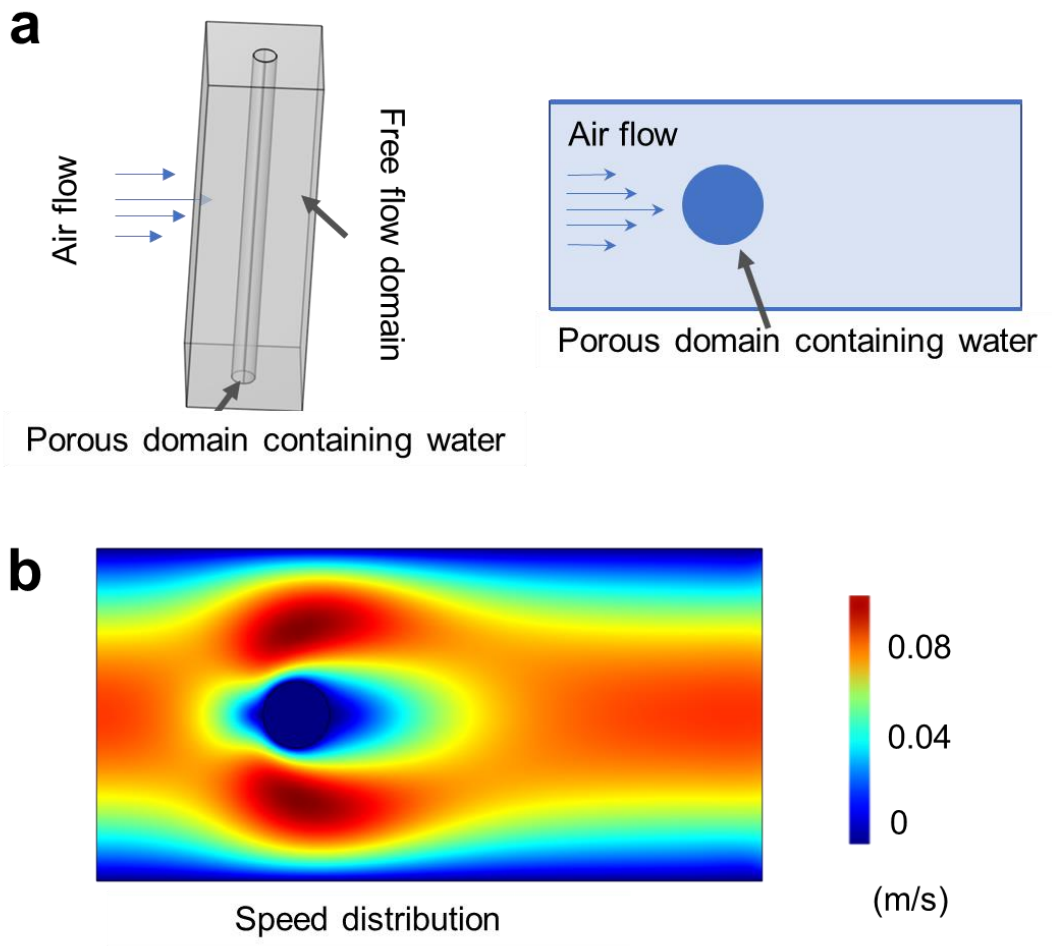

Fig S9. a) A full-scale model was used to simulate the drying process of hydrogel fiber in the stage of air drying. b) The wind speed distribution near the surface of hydrogel fiber.

The Reynolds number (*Re*) of this system could be approximately calculated as below

$$Re = \rho v \frac{d}{\mu} \quad (2)$$

Here, the ρ is the density of air (~1.2 kg/m^3), v is the flow speed (set as 0.05 m/s), d is the characteristic linear dimension (for cylinders is the diameter, ~0.001 m) and μ is the dynamic viscosity of air (~1.85×10^{-5} Pa·s). Thus the *Re* in our system is around 0.3, revealing the flow of air is the stable laminar flow.

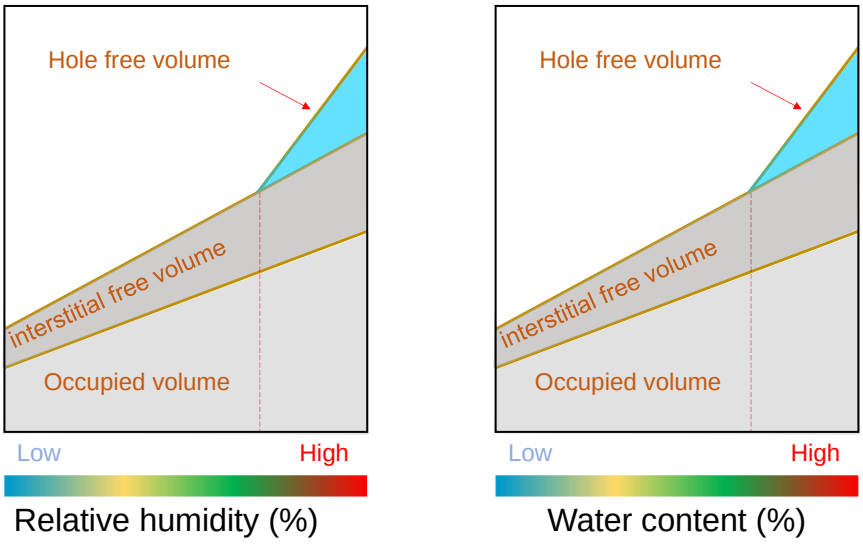

Fig S10. The free volume induced by water sorption in xerogel fibers.

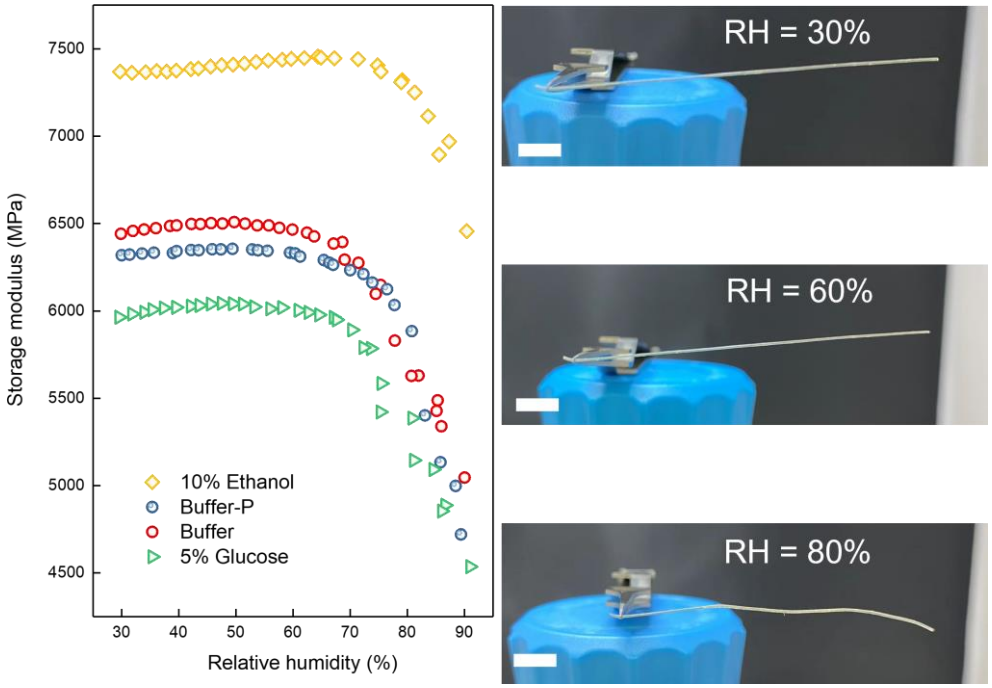

Fig S11. The storage modulus of xerogel fibers using humidity sweep method and the snapshots of xerogel fibers under different relative humidity. Scale bar: 1 cm.

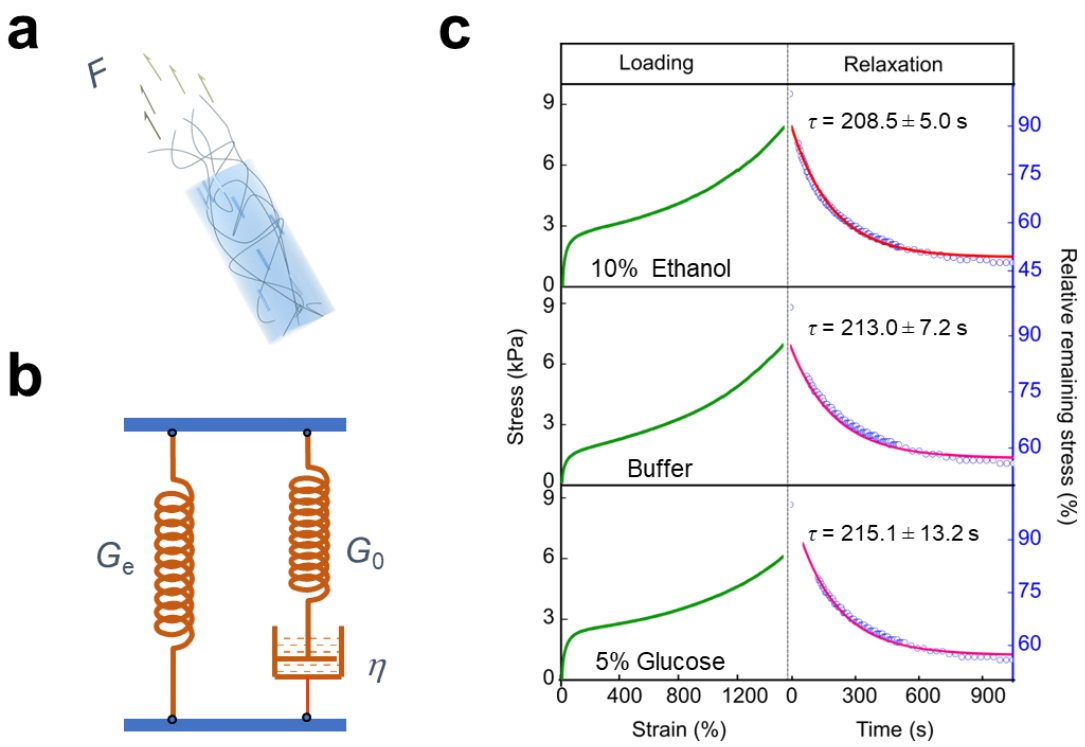

Fig S12. a) The schematic illustration of uniaxial tensile. b) A typical Voigt-Kelvin model to describe the stress relaxation process of crosslinked polymer. c) The typical stress-relaxation curves of hydrogel fibers.

The total stress (G_{all}) is the sum of both parts:

$$G_{all} = G_e + G_0 e^{-\frac{t}{\tau}} \quad (3)$$

Here G_e and G_0 are the stress of spring and dashpot, t and τ are the time after starting relaxation and τ is called relaxation time, which is the important material parameter used to characterize viscoelastic materials. Considering these three hydrogels were prepared using different solvents, we used the initial stress (t = 0) to normalized the stress relaxation and shown as relative remining stress. As the initial strain rate applied to establish a constant strain same for these tests, stress relaxation tests were conducted and demonstrated the similar characterizations. All three hydrogels behaved typical viscoelasticity features, in both loading and relaxation process. Using Eq. (3) the stress relaxation process was simulated, the coefficient of determination (R^2) of three samples was higher than 99.5%. Therefore, it was appropriate that we used Voigt-Kelvin model to describe the actual behavior of CNC hybrid hydrogels in air drying steps.

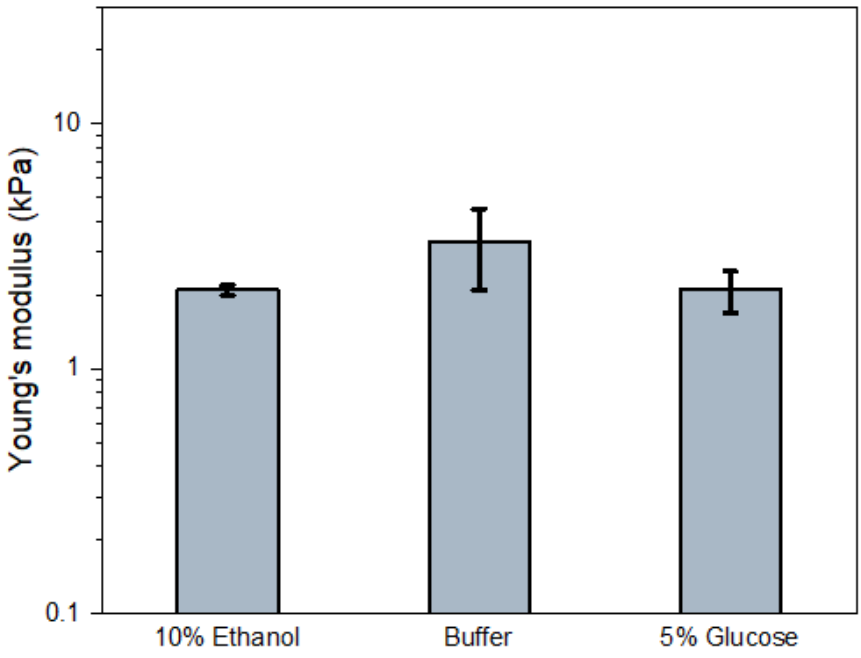

Fig S13. Young's modulus of various samples.

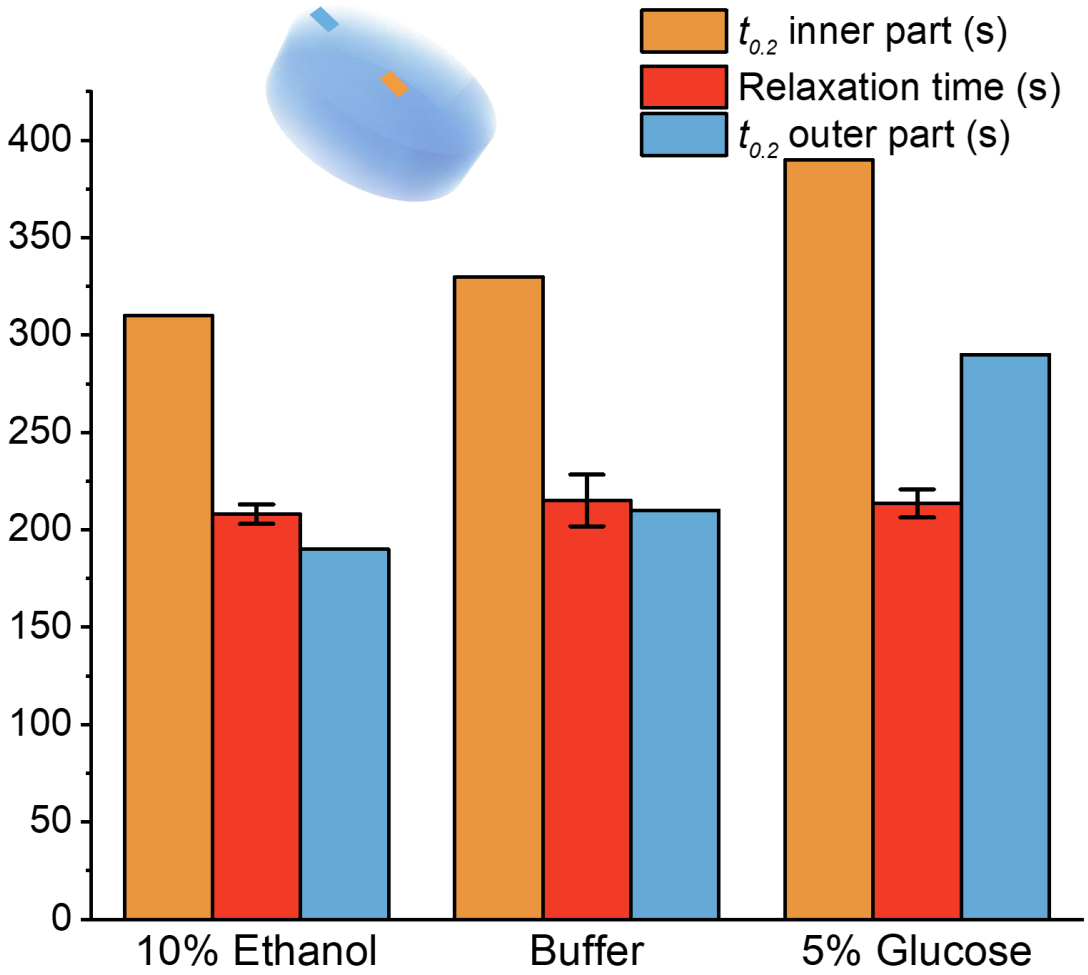

Fig S14. Relaxation times of various samples and the time point when the water content was less than 20% for their inner and outer parts (according the simulation results). Inset: selected area of inner part and outer part for analysis.

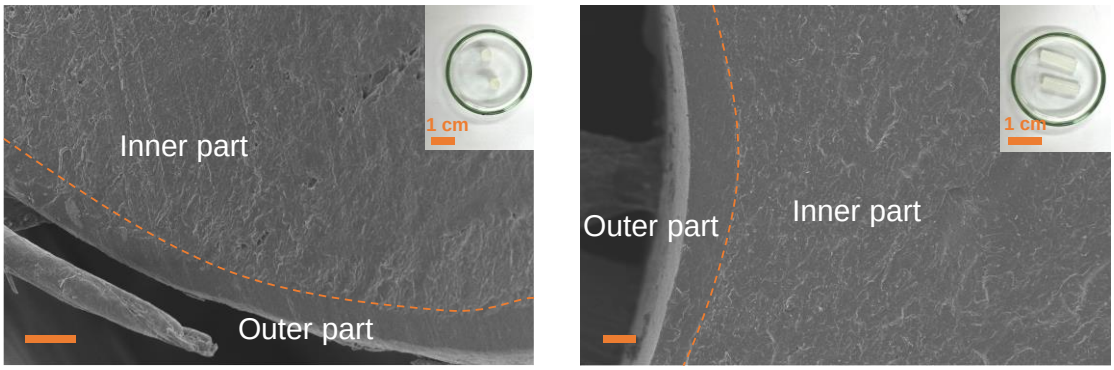

Fig S15. The heterogeneous structures were found in obtained xerogel fibers without stretching. Left) The virgin hydrogels were placed vertically. Right) The virgin hydrogels were placed horizontally. Scale bar: 10 μm. Insets: the original status of hydrogels. Here, the buffer samples were used.

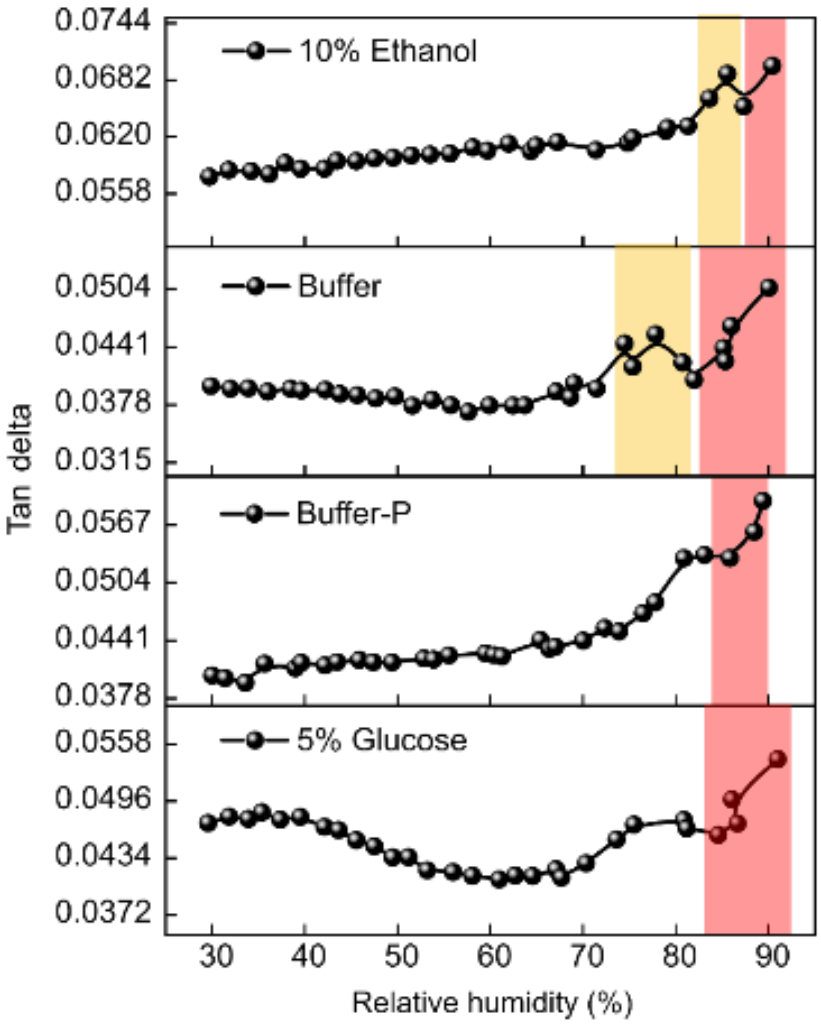

Fig S16. Loss factors of four different xerogel fibers as measured from humidity sweep tests on DMTA. The second order transition (brown region) was found in both 10% ethanol and buffer fibers, which were induced by the existence of an outer layer.

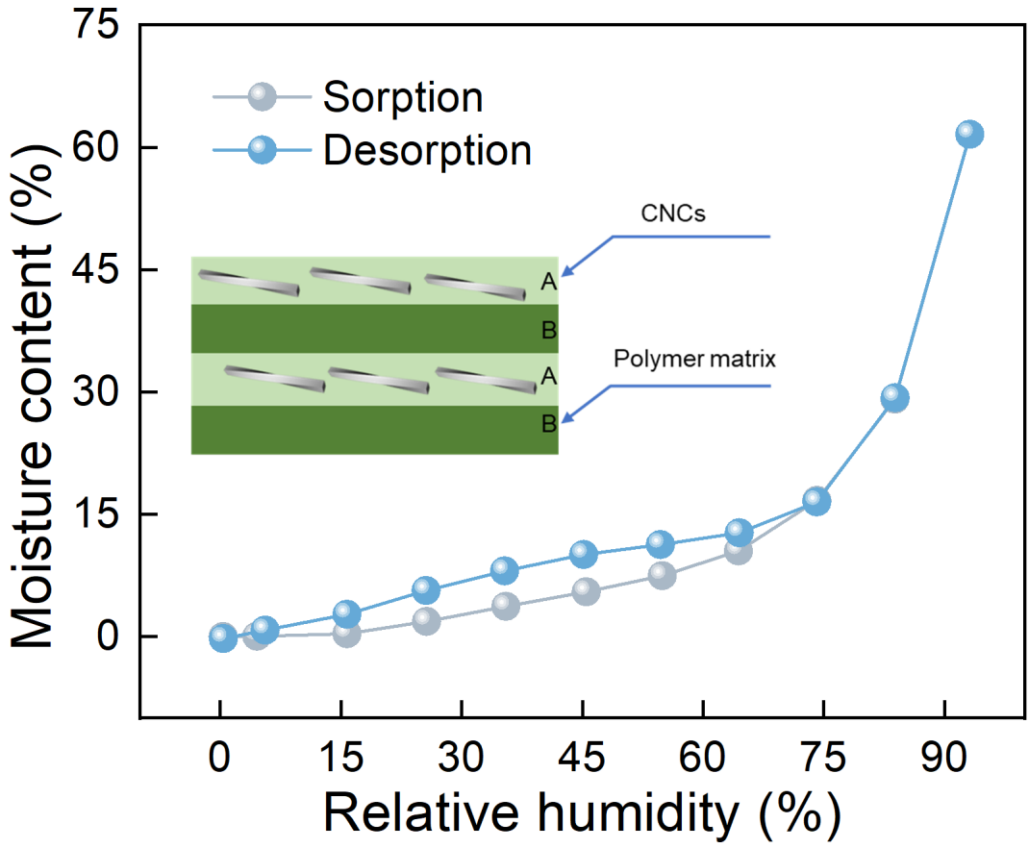

Fig S17. The typical isothermal sorption-desorption curves of xerogel fibers. The type B hysteresis loops are associated with slit shaped pores.

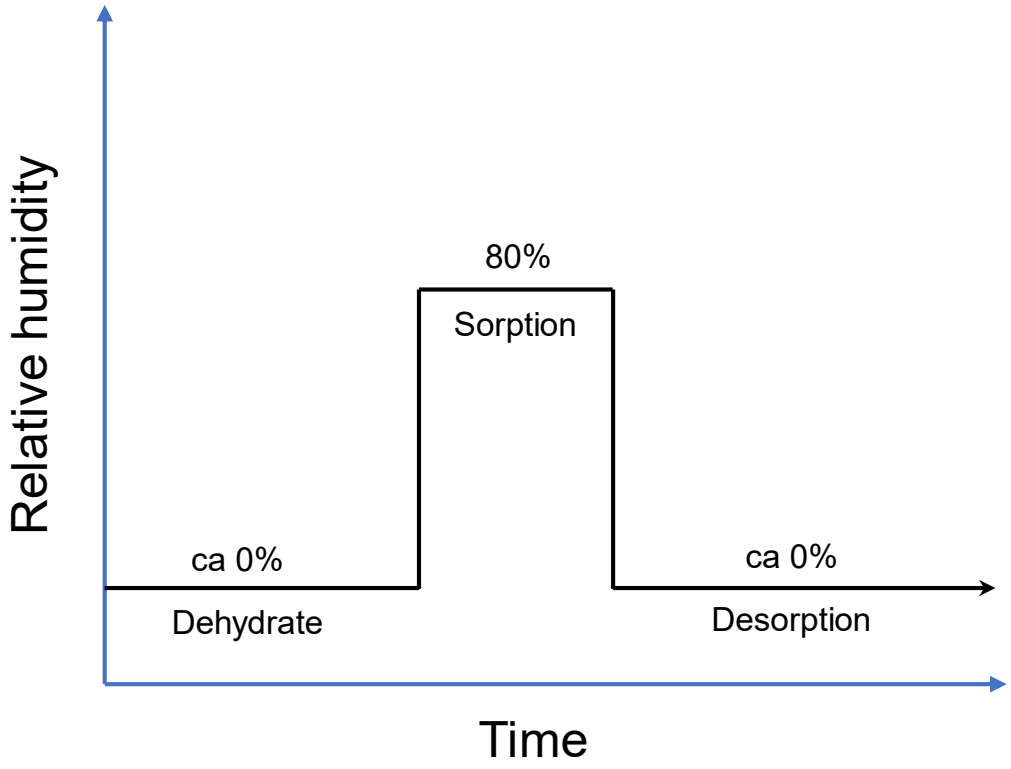

Fig S18. Method to determine the sorption-desorption properties of xerogel fiber under consistent temperature.

Table S2. Aspect ratio of different samples

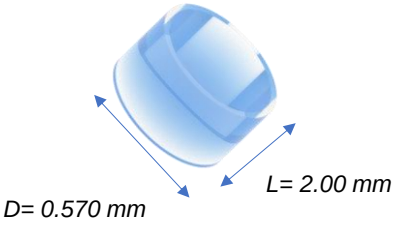	*L*/*D* = 3.5
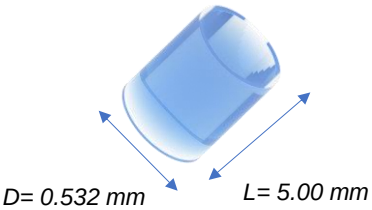	*L*/*D* = 9.4
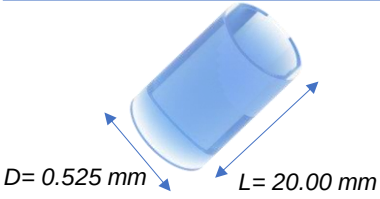	*L*/*D* = 38.1

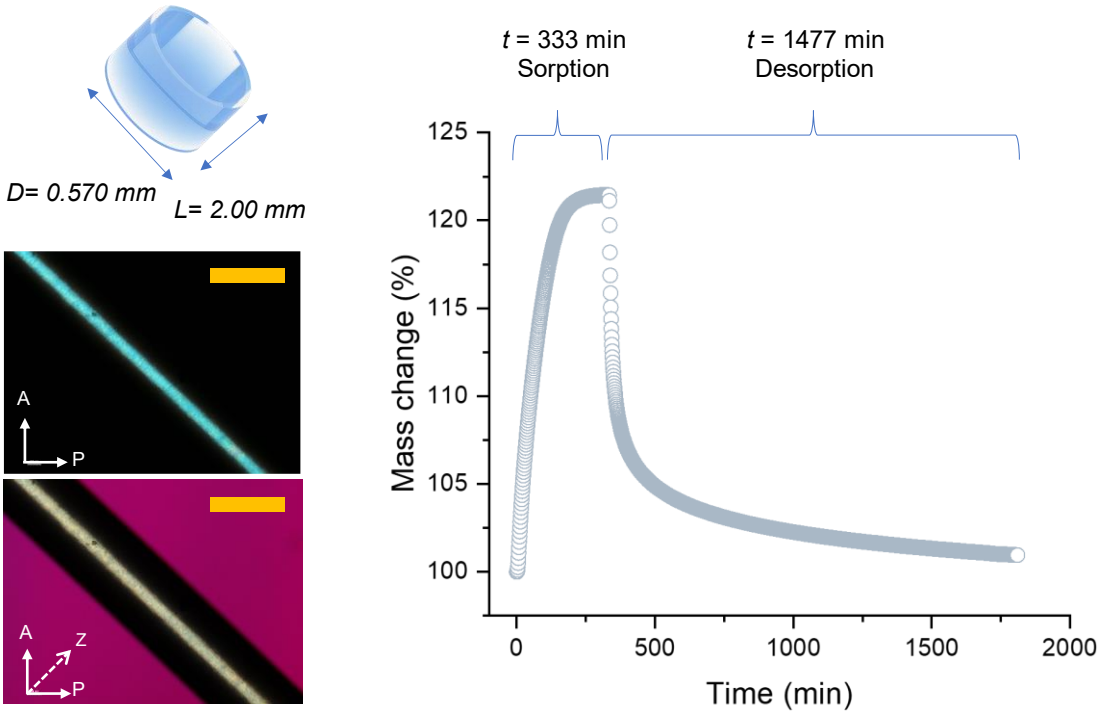

Fig S19. Sorption-desorption behavior of xerogel fiber (formed in buffer, length 2.00 mm) left) The geometric shape and optical properties of xerogel. right) Typical water vapor sorption-desorption curve of xerogel. Scale bar: 500 μm.

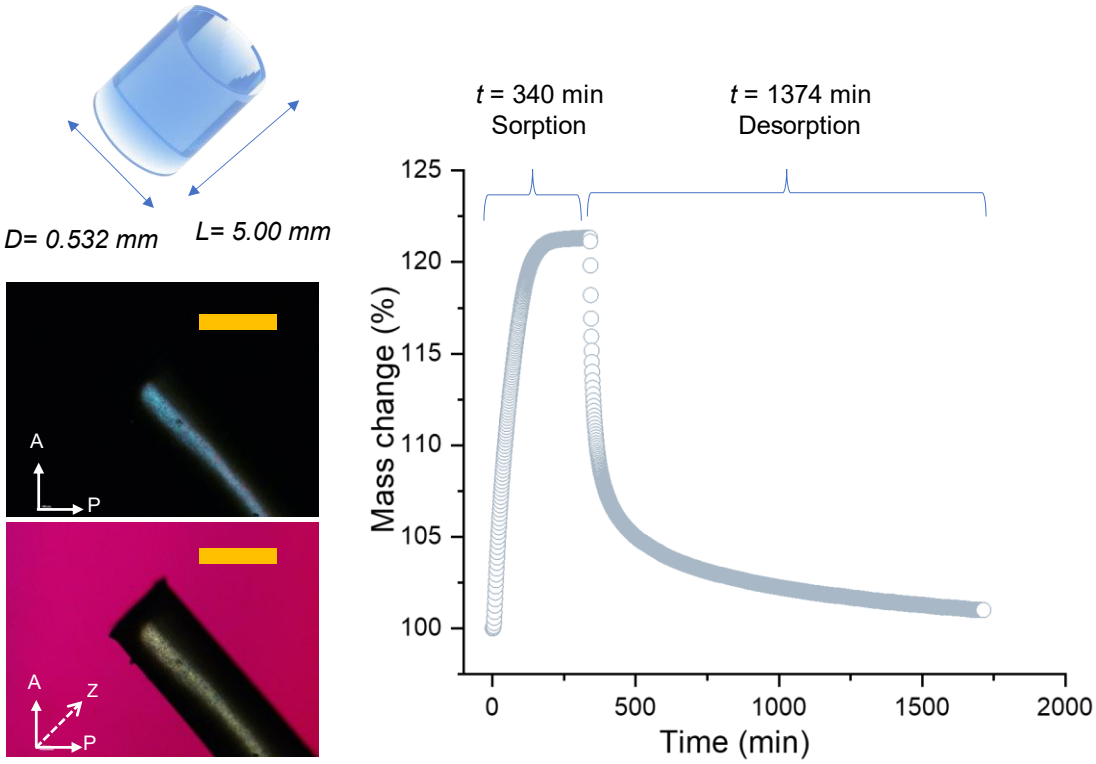

Fig S20. Sorption-desorption behavior of xerogel fiber (formed in buffer, length 5.00 mm) left) The geometric shape and optical properties of xerogel. right) Typical water vapor sorption-desorption curve of xerogel. Scale bar: 500 μm.

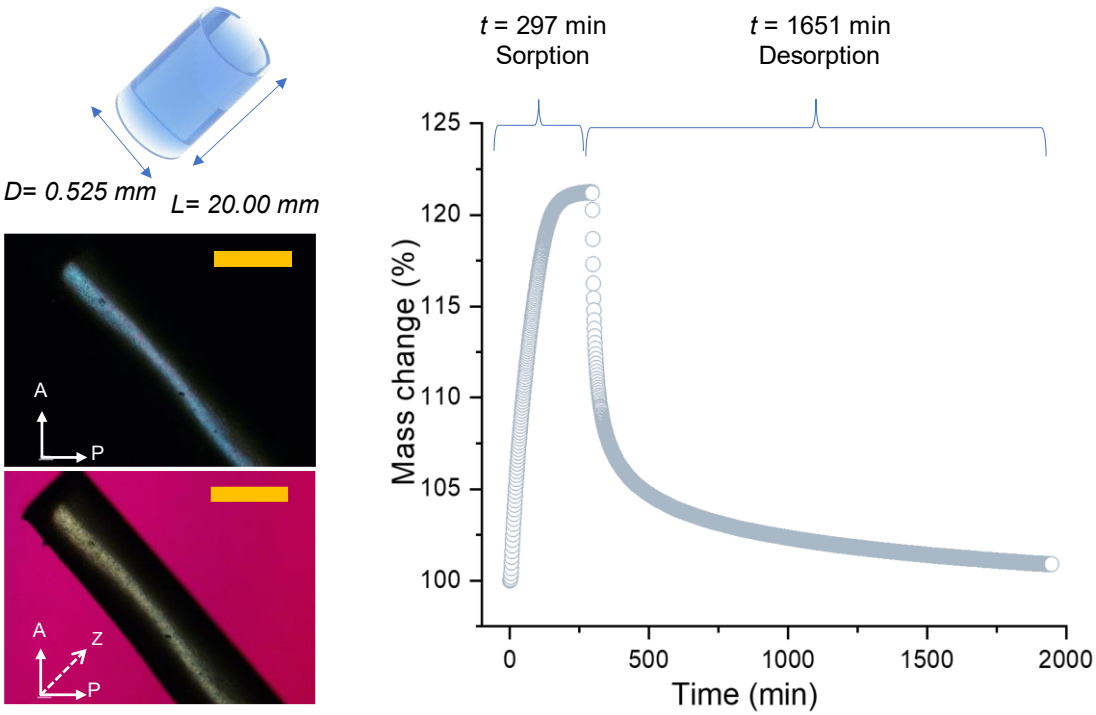

Fig S21. Sorption-desorption behavior of xerogel fiber (formed in buffer, length 20.00 mm) left) The geometric shape and optical properties of xerogel. right) Typical water vapor sorption-desorption curve of xerogel. Scale bar: 500 μm.

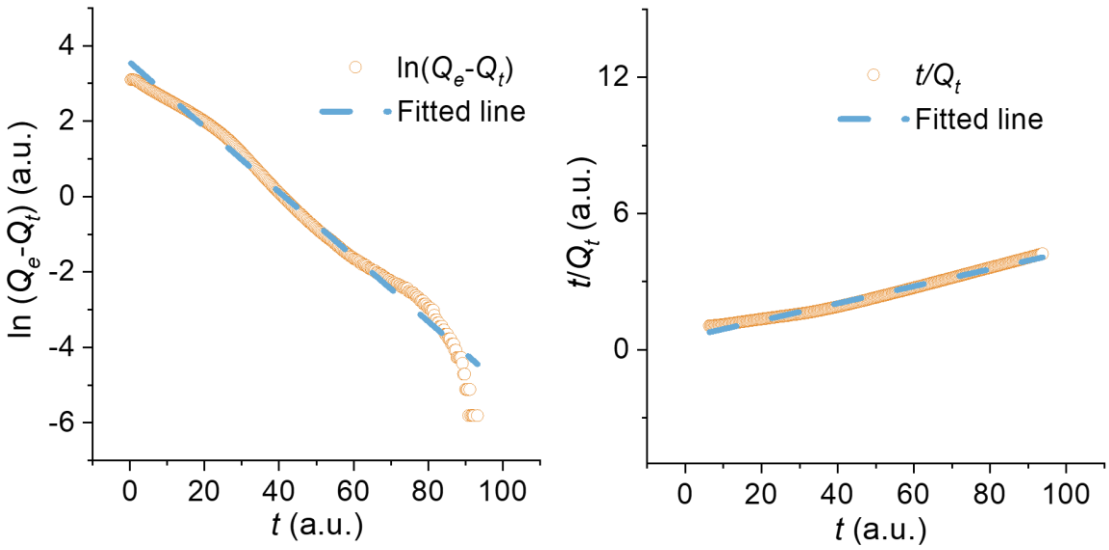

Fig S22. left) Pseudo-first-order and right) Pseudo-second-order adsorption kinetic fitting curves of the typical sorption curves.

Table S3. Kinetic parameters for sorption of water vapor by hybrid xerogel fibers

Number		1	2	3
		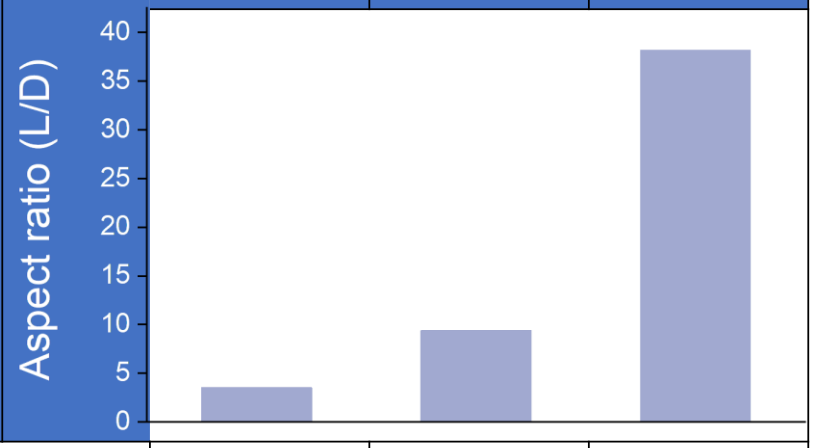		
Experimental sorption capacity		21.43	21.24	21.32
Pseudo 1st-order sorption kinetics	Q_e	32.52	24.43	24.48
	K_1	0.1178	0.0739	0.0627
	R^2	0.9638	0.9873	0.9933
Pseudo 2nd-order sorption kinetics	Q_e	28.36	27.93	25.37
	K_2	0.0021	0.0019	0.002
	R^2	0.9837	0.9824	0.9874
Weber and Morris intraparticle diffusion	K_{id1}	0.1626	0.2595	0.0646
	K_{id2}	3.9411	3.5212	3.0028
	K_{id3}	0.2157	0.1679	0.0839

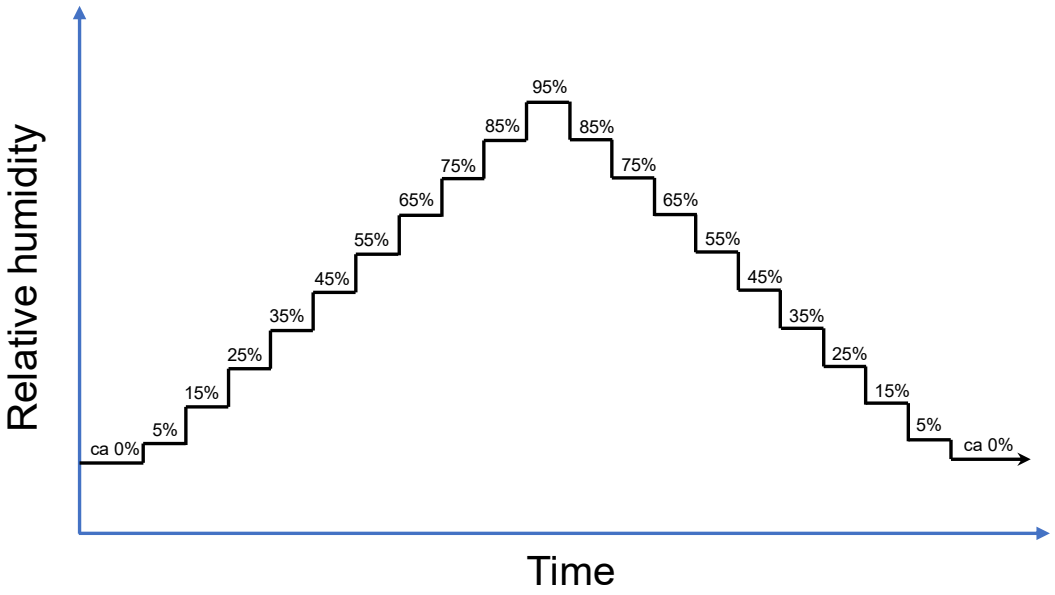

Fig S23. A typical sorption-desorption method to determine the sorption isotherm of xerogel fibers.

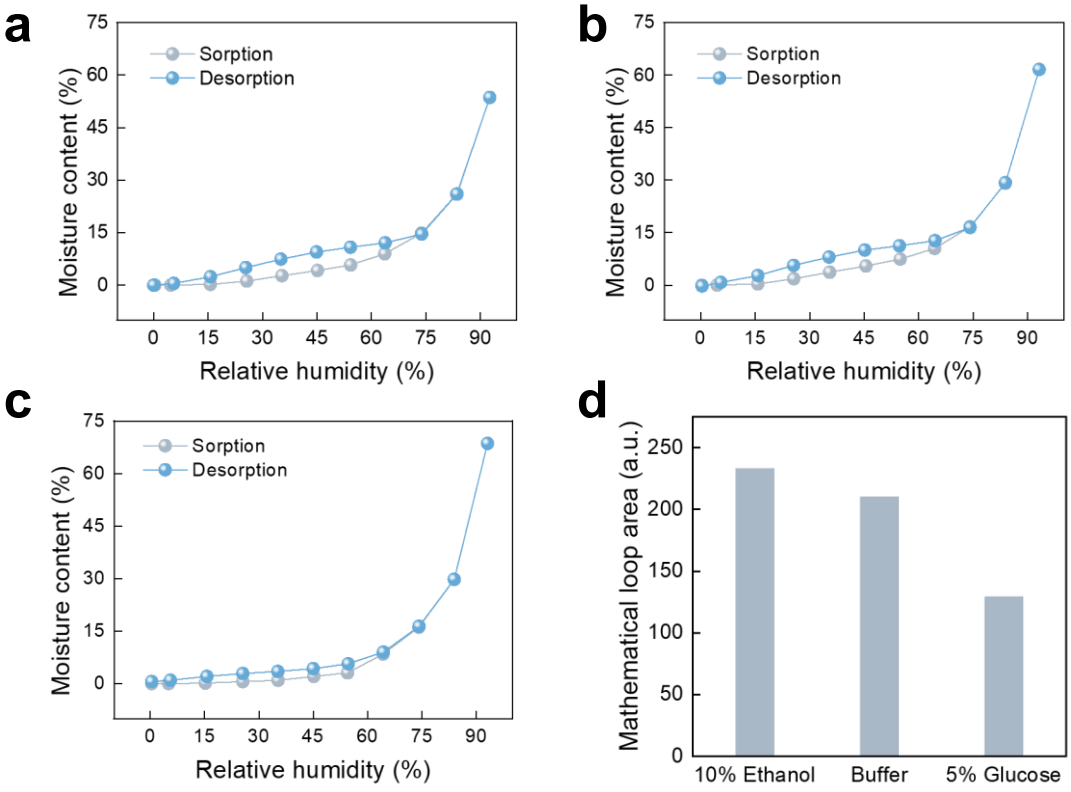

Fig S24. Sorption and desorption isotherms of xerogel fibers. a) 10% ethanol. b) Buffer. c) 5% glucose. d) The mathematic area of hysteresis loop of various samples.

Reference:

1. S. Xu, S. Cai, Z. Liu, Thermal Conductivity of Polyacrylamide Hydrogels at the Nanoscale. *ACS Applied Materials & Interfaces* **10**, 36352-36360 (2018).
2. S. Davidson, M. Sherar, Measurement of the thermal conductivity of polyacrylamide tissue-equivalent material. *International journal of hyperthermia* **19**, 551-562 (2003).
3. C. A. Grattoni, H. H. Al-Sharji, C. Yang, A. H. Muggeridge, R. W. Zimmerman, Rheology and permeability of crosslinked polyacrylamide gel. *Journal of colloid and interface science* **240**, 601-607 (2001).
4. A. F. Prokop *et al.*, Polyacrylamide gel as an acoustic coupling medium for focused ultrasound therapy. *Ultrasound in medicine & biology* **29**, 1351-1358 (2003).
5. C. Raymond, S. Ronca, "Relation of structure to electrical and optical properties" in Brydson's Plastics Materials. (Elsevier, 2017), pp. 103-125.